Environ Geochem Health (2012) 34:527–538
DOI 10.1007/s10653-011-9438-7

ORIGINAL PAPER

Pyrite-driven reactive oxygen species formation in simulated lung fluid: implications for coal workers' pneumoconiosis

Andrea D. Harrington · Shavonne Hylton · Martin A. A. Schoonen

Received: 14 April 2011 / Accepted: 27 September 2011 / Published online: 12 October 2011

Abstract The origin of coal worker's pneumoconiosis (CWP) has been long debated. A recent epidemiological study shows a correlation between what is essentially the concentration of pyrite within coal and the prevalence of CWP in miners. Hydrogen peroxide and hydroxyl radical, both reactive oxygen species (ROS), form as byproducts of pyrite oxidative dissolution in air-saturated water. Motivated by the possible importance of ROS in the pathogenesis of CWP, we conducted an experimental study to evaluate if ROS form as byproducts in the oxidative dissolution of pyrite in simulated lung fluid (SLF) under biologically applicable conditions and to determine the persistence of pyrite in SLF. While the rate of pyrite oxidative dissolution in SLF is suppressed by 51% when compared to that in air-saturated water, the initial amount of hydrogen peroxide formed as a byproduct in SLF is nearly doubled. Hydroxyl radical is also formed in the experiments with SLF, but at lower concentrations than in the experiments with water. The formation of these ROS indicates that the reaction mechanism for pyrite oxidative dissolution in SLF is no different from that in water. The elevated hydrogen peroxide concentration in SLF suggests that the decomposition, via the Fenton mechanism to hydroxyl radical or with Fe(III) to form water and molecular oxygen, is initially inhibited by the presence of SLF components. On the basis of the oxidative dissolution rate of pyrite measured in this paper, it is calculated that a respirable two micron pyrite particle will take over 3 years to dissolve completely.

Keywords Pyrite · Oxidative dissolution · Reactive oxygen species · Coal workers' pneumoconiosis

A. D. Harrington (✉) · S. Hylton · M. A. A. Schoonen
Department of Geosciences, Stony Brook University, Stony Brook, NY 11794-2100, USA
e-mail: ADHarrin@ic.sunysb.edu

Background

Coal mining represents an occupational health burden that is likely to increase globally. Even with the emergence of alternative energy resources, coal continues to be a major energy supply worldwide and its demand and production are still on the rise. Currently, 45% of the electricity in the United States is derived from coal-burning power plants (USEIA 2011). The 2003 Basic Energy Sciences Advisory Committee forecasts that by the year 2050, the energy requirements for Earth's population will double. Most of this increased energy demand will likely be met with fossil fuels, and coal in particular. More specifically, according to the United States Energy Information Administration, world coal consumption will increase by 49% from 2006 to 2030 (127.5 quadrillion Btu to 190.2 quadrillion Btu) (USEIA 2009). Much of the recent increase in production to meet the growing global energy demand has come by expansion of coal mining in Asia. Whereas in the United States coal

mining has been transformed into a highly mechanized operation, coal mining in less developed countries, such as China, is a labor-intensive operation.

The most prevalent work-related ailment among coal miners is coal workers pneumoconiosis (CWP). Coal miners account for no more than 0.02% of the US population, but represent half of the pneumoconiosis deaths during the last decade of the twentieth century (NIOSH 2003), which points to the high prevalence of CWP among coal miners. Originally thought to be a variant of silicosis, CWP has recently been linked to pyrite. An epidemiological study has demonstrated a correlation between the bioavailable iron (BAI) content in coal and the prevalence of CWP in miners (Huang et al. 2005). BAI is defined as the amount of iron released over a 3 h period in 10 mM phosphate solution at room temperature and a pH of 4.5 (Huang et al. 1998, 2005). The results of a recent experimental study suggest that the pyrite content of the coal, which can be as high as 5% by weight, is the underlying factor that causes the relationship between BAI and the prevalence of the disease (Cohn et al. 2006b). Furthermore, a study conducted in Great Britain showed that tissue recovered from pneumoconiotic lungs of deceased coal miners has abnormally high amounts of iron-enriched material (Bergman and Casswell 1972), consistent with the notion that exposure to iron minerals associated with coal plays a role in the pathogenesis of CWP. Pyrite and pyrite-bearing coal have recently been shown to spontaneously generate ROS when placed in water (Cohn et al. 2005, 2006c). On the basis of these results and additional research with pyrite-bearing coal, it has been suggested that the inhalation of iron-bearing dust may be responsible for a chronic elevated level of reactive oxygen species (ROS) production in lung tissue. This, in turn, may contribute to the pathogenesis of the disease (Cohn et al. 2006b). However, these conclusions were based on experiments conducted in water. The goals of this study are to determine the oxidative dissolution rate of pyrite in simulated lung fluid (SLF) and to evaluate if pyrite particles can generate ROS in SLF.

Simulated lung fluid is a proxy for the extracellular fluid lining the surface of the alveolar epithelium (Eastes et al. 1995; Mattson 1994; Potter and Mattson 1991). This area of the lungs accumulates all of the respirable particulates and it is the primary environment for dissolution before phagocytosis can occur (for phagocytosis to occur a particle must be less than 15–20 μm in size) (Cannon and Swanson 1992; Bauer et al. 1997). While phagocytosis is the primary method of clearance for respirable particles, "particle overload" can occur if the inhalation rate is greater than the alveolar clearance rate (Renwick et al. 2001; Morrow 1988). Under conditions of particle overload, the clearance rate due to phagocytosis can be slowed or halted (Oberdorster 1995). Hence, it is useful to experimentally determine the rate of dissolution of environmentally relevant particles, such as pyrite, in SLF. On the basis of experimentally determined dissolution rates, it is possible to estimate the total time it takes to dissolve a particle of a given size upon inhalation.

A range of SLF formulations with different levels of complexity have been used in studies designed to evaluate the persistence/dissolution of particulate matter. Gamble's description of the composition of extracellular lung fluid is the basis for the formulation of SLF used here and in most other studies (Gamble 1942). There are two different approaches to approximate natural extracellular lung fluid. One approach is to use a solution that is principally sodium chloride with both additional inorganic (bicarbonate, ammonium, phosphate) and organic components (glycine and citrate). The solution is kept at 37°C and buffered at pH 7.4 by bubbling a 5% CO_2–air gas mixture through it. The drawback of this approach is that it does not capture the complexity of lung fluid as it lacks proteins, fatty acids, antioxidants, and other complex biomolecules. This shortcoming is overcome in the second approach by adding various complex biomolecules to the "simple" SLF.

A simple SLF is often used, however, to study the biopersistence of particulate matter in vitro (Lehuede et al. 1997; Wragg and Klinck 2007; de Meringo et al. 1994; Berlinger et al. 2008; Oze and Solt 2010; Metzger et al. 1997; Jurinski and Rimstidt 2001; Kanapilly 1977; Gamble 1942; Bauer et al. 1997). It has been shown that the absence of proteins and antioxidants has no marked effect on the dissolution rate of natural or man-made contaminants (Jurinski and Rimstidt 2001; de Meringo et al. 1994), as long as the temperature and pH are kept at biologically relevant conditions. For example, the dissolution rate of talc at 37°C and a pH of 7.4 does not change when the fluid is varied from a very simple phosphate-buffered solution to a more complex SLF (Jurinski and

Rimstidt 2001). In the present study, the rate of pyrite oxidative dissolution was determined in both a simple SLF (see Table 1) and one with added proteins and fatty acids. While a simple SLF formulation does not capture the full complexity of natural lung fluid, its simplicity makes it possible to evaluate the full extent to which particulates can generate ROS. The addition of more complex biomolecules provides additional pathways for superoxide, hydrogen peroxide, and hydroxyl radical to react, which decreases the steady state ROS concentrations. For example, as demonstrated in this study, the addition of a mixture of proteins and fatty acids (beractant, Survanta®; Table 2) lowers the hydrogen peroxide concentration in an experiment in which pyrite was dispersed in SLF lacking complex biomolecules.

The formation of ROS in pyrite slurries is a byproduct of oxidative dissolution of pyrite in air-saturated fluids. The equations below represent simplified reactions known to occur in natural waters. Although the systems complexity increases in vivo, the simplified reaction paths remain applicable. The oxidant can be molecular oxygen (reaction 1) and/or dissolved ferric iron (reaction 2). Dissolved ferric iron can be formed in a pyrite slurry by the oxidation of ferrous iron (reaction 3).

$$2FeS_2 + 7O_2 + 2H_2O \rightarrow 2Fe^{2+} + 4SO_4^{2-} + 4H^+ \quad (1)$$

$$FeS_2 + 14Fe^{3+} + 8H_2O \rightarrow 15Fe^{2+} + 2SO_4^{2-} + 16H^+ \quad (2)$$

$$2Fe^{2+} + 1/2O_2 + 2H^+ \rightarrow 2Fe^{3+} + H_2O \quad (3)$$

The oxidative dissolution of pyrite allows for iron to be released into solution as ferrous iron. When ferrous iron interacts with dissolved molecular oxygen, the Haber–Weiss reaction mechanism sequence is initiated. This reaction sequence leads to the formation of hydrogen peroxide with superoxide acting as an intermediate (reactions 4, 5).

$$Fe^{2+} + O_2 \rightarrow Fe^{3+} + {}^{\cdot}O_2^- \quad (4)$$

$$Fe^{2+} + {}^{\cdot}O_2^- + 2H^+ \rightarrow Fe^{3+} + H_2O_2 \quad (5)$$

The existence of hydrogen peroxide allows for the formation of another ROS, hydroxyl radical, via the Fenton reaction (reaction 6). The fate of hydrogen peroxide depends, however, on the relative availability of ferrous and ferric iron. While a reaction with ferrous iron leads to the formation of hydroxyl radical, a reaction with ferric iron leads to decomposition of hydrogen peroxide into water and oxygen (reaction 7). In this respect, ferric iron acts similar to catalase (Schoonen et al. 2010).

$$H_2O_2 + Fe^{2+} \rightarrow Fe^{3+} + OH^- + {}^{\cdot}OH \quad (6)$$

$$3H_2O_2 + 2Fe^{3+} \rightarrow 2Fe^{2+} + 2H_2O + 2O_2 + 2H^+ \quad (7)$$

It is expected that pyrite oxidative dissolution in SLF differs from pyrite oxidative dissolution in water, because dissolved phosphate has been shown to slow the rate of pyrite oxidative dissolution (Elsetinow et al. 2001) and carboxylic acids have been shown to sorb onto its surface (Bebie and Schoonen 2000). Sorption of carboxylic acids could affect the reaction mechanism and dissolved carboxylic acids may suppress the concentration of hydroxyl radical by complexing

Table 1 Composition of simulated lung fluid

Components	Concentration (mM)
Na^+	150.7
Ca^{2+}	0.197
NH_4^+	10.0
$H_2CNH_2CO_2H$ (glycine)	5.99
Cl^-	126.4
SO_4^{2-}	0.5
HCO_3^-	27.0
HPO_4^{2-}, $H_2PO_4^-$	1.2
$[HOC(CH_2CO_2)_2CO_2]^{3-}$ (citrate)	0.2

Modified Gamble's solution from Bauer et al. (1997)

Table 2 Composition of Survanta® (beractant)

Components	Concentration (mg/mL)	Details
Phospholipids	25	Including 11.0–15.5 disaturated phosphatidylcholine
Triglycerides	0.5–1.75	NA
Free fatty acids	1.4–3.5	NA
Protein	<1	Two hydrophobic, low molecular weight (SP-B and SP-C)

Suspended in a 0.9% sodium chloride solution

Drugs.com Updated: 2011 September 19; Cited 2011 September 20

ferrous iron and preventing the Fenton reaction (reaction 6) or by scavenging the radical.

Experimental methods

Batch experiments

Batch oxidative dissolution experiments were performed on slurries of pyrite (Huanzala, Peru) in a 250 mL- glass, magnetically stirred vessel equipped with a water jacket (Ace Glass™). The vessel was fitted with a cover containing four ports to allow for insertion of a pH probe, a dissolved oxygen probe, a titrant buret, a gas inlet and outlet, and a sampling tube. Both in situ and *ex situ* measurements were performed. The in situ measurements—temperature, dissolved oxygen and pH—were used in real time to keep the conditions in the mineral slurry saturated with air, at pH 7.4, and at 37°C. The *ex situ* measurements—hydrogen peroxide, ferrous iron and sulfate—were used to determine the rate of pyrite oxidative dissolution and to determine the concentration of hydrogen peroxide throughout the course of the experiments.

X-ray fluorescence spectroscopy (Bruker S4 Pioneer) showed that the pyrite used in these experiments contained little to no impurities. Before use, the pyrite was crushed in an agate mill and sieved to less than 38 μm in order to obtain a suitable size fraction. The starting material was subsequently cleaned using a 0.1 M HCl solution to remove iron hydroxide and/or iron oxy-hydroxide patches from the surface and stored under vacuum in an anaerobic glove bag. The specific surface area of the pyrite, determined with a Quantachrome NOVA 5-point BET analyzer, was 1.923 m^2/g. The average diameter is estimated on the basis of the specific surface measurement to be 0.62 μm.

The temperature of the reaction vessel was controlled via a constant-temperature circulating water bath equipped with a thermostat-controlled heater. Kept at 37°C, the experiment was further monitored using a dissolved oxygen probe equipped with a thermistor (HACH™ LDO probe). This same probe's primary use was to continuously monitor the dissolved oxygen (DO) content in the slurry. The pH was monitored using a Titroline Alpha™ pH–stat equipped with a single junction, gel-filled electrode (Fisher™). The electrode was calibrated with standard NIST-traceable pH buffer solutions before the start of the experiment.

In order to evaluate the effect of SLF on the oxidative dissolution rate of the pyrite, separate replicate batch experiments were conducted with deionized (DI) water and SLF. In both experiments, molecular oxygen was the oxidant (some ferric iron is likely to have formed in the system, but at the pH of the experiments (7.4) very little dissolved ferric iron is expected to be present). The vessel was charged at the start of each experiment with 170 mL of the desired liquid (DI water or SLF), which was allowed to warm to 37°C and reach a pH of 7.4 before the pyrite was added ($\sim$1 h). The DO content was also allowed to stabilize at $\sim$6.5 mg/L, which represents saturation at the temperature of the experiments. Although considered a high dose, a pyrite loading of 0.004 m^2/mL was used for each experiment (353 mg/170 mL) allowing for comparison with previous work. The reaction vessel was covered with aluminum foil throughout the experiment to block out the effect of light on pyrite oxidative dissolution, which has been shown to increase the oxidative dissolution rate (Schoonen et al. 2000). Samples were taken over the course of the experiment for iron, sulfate and hydrogen peroxide analyses.

For the majority of the experiments performed in SLF, the pH was kept constant using the buffering capacity of the SLF in conjunction with CO_2. The CO_2 was delivered to the system via a tank containing 10% CO_2 in compressed air and fed into the system using a bubbler. The flow rate of the CO_2 gas was adjusted so that the pH of the fluid was maintained within $\pm$0.1 of 7.4. Fresh SLF was prepared before each experiment using the procedure of Bauer et al. (1997) which is a simple SLF (Kanapilly 1977). Briefly, individual sodium dihydrogen phosphate monohydrate, sodium citrate dihydrate, sulfuric acid, ammonium chloride and calcium chloride solutions were made. The latter two intermediate solutions were filtered using 0.22-μm membrane slip-on filter before being added to the final container. The above solutions were mixed with a solution of sodium chloride, sodium bicarbonate, sodium carbonate and glycine in a calibrated glass flask. Given the short duration of the experiments, formaldehyde—a bactericide—was not added to the SLF as prescribed by Bauer et al. (1997) (Table 1). The reagents used were of the highest quality, although we cannot exclude that they contain some

trace amounts of metal. However, given their consistent use throughout the course of the experimental process and their trace levels compared to the amount of iron released by the pyrite, their presence is not expected to affect the conclusions. All SLF solutions were used within 24 h of preparation. The SLF solutions were stored in the dark at 4°C between preparation and use in the experiments. The effect of a more complex SLF solution on the pyrite oxidative dissolution rate was evaluated by adding two separate 6 μg/mL aliquots of Survanta® to a batch experiment with the simple SLF (Wang et al. 2010). By determining the rate of sulfate formation before and after the additions of Survanta®, we were able to calculate the pyrite oxidative dissolution rate in simple SLF and the rate with added proteins and fatty acids, while all other conditions in the experiment remained constant. The airflow into the reaction vessels was kept at 120 mL/min. For experiments performed with DI water at 37°C, a 0.1 M NaOH solution was automatically titrated into the vessel to maintain the pH within a desirable range (7.4 ± 0.4). Tank gas was not used for these experiments; air was simply bubbled through the system via an air pump (Secondnature Challenger I). The air stream from the pump was first passed through a KOH solution to remove CO_2, which is necessary to keep the pH under control.

The concentration of hydrogen peroxide was determined in aliquots withdrawn from the vessel using the leuco crystal violet (LCV) method as previously reported (Cohn et al. 2005), with some minor modification to compensate for the high buffering capacity of the SLF used in the experiments. In short, this modified method consists of pipetting 500 μL Na ethylenediaminetetraacetic acid (EDTA) into a polystyrene cuvette (the EDTA is added to prevent the decomposition of hydrogen peroxide in the sample via the Fenton reaction by chelating free iron). Next, 100 μL of HRP and LCV reagent are added, followed by a pH buffer, KH_2PO_4, to ensure the pH is at/near the optimal range of 4.2. Finally, 700 μL DI water was added. This mixture of reagents was prepared in the cuvettes before a 500 μL sample was withdrawn by syringe from the vessel for hydrogen peroxide analysis. The sample was filtered using a 0.22-μm membrane slip-on filter before adding it to the reagents in the cuvette. After incubation in the dark for 10 min, the absorbance of the purple complex was measured using a HACH DR/4000 UV/vis spectrometer at a wavelength of 590 nm. Standards were made in order to determine the concentration of hydrogen peroxide in the samples. The concentration of dissolved ferrous iron remaining in the slurry at the end of the experiment was quantified by means of a HACH DR/4000 UV/vis spectrometer, using Hach™ Ferrozine method (Hach™ method 8147). The samples were analyzed for sulfate, a proxy for pyrite dissolution, using an automated ion chromatograph (Dionex™ DX 500) equipped with an AS4A-SC column.

Fluorescence assay procedures

The effect of SLF on the formation of hydroxyl radical was determined in a separate set of experiments apart from the batch experiments described above. The experiments followed a previously published protocol for the determination of hydroxyl radical in mineral slurries (Cohn et al. 2009). Natural pyrite from Huanzala, Peru, was purchased from Wards, crushed in an agate mill, sieved to less than 38 μm and stored under anoxic conditions until use. Using a five-point N_2 adsorption BET, the specific surface area of the pyrite was determined to be 1.25 m^2/g. The average particle size was one micron based on the specific surface area measurement. SLF was prepared as described above. The slurries (one in water and one in SLF) were spiked with the fluorogenic probe 3′-(*p*-aminophenyl) fluorescein (APF) (Dorr et al. 2003) at a concentration of 10 μM. For the experiments performed without pyrite, the same concentration of APF was injected as well as a 10 mM solution of ferrous ammonium sulfate heptahydrate or a 10 mM solution of ferric sulfate pentahydrate (one in water and one in SLF each). The slurries/samples were subsequently incubated for 24 h at 25°C. During the incubation periods, the slurries were placed on a Barnstead/Thermolyne Labquake rotating mixer to keep the minerals in suspension.

After the incubation period, all samples were measured in 4-mL methylcrylate fluorescence cuvettes on a Turner Barnstead spectrofluorometer with excitation and emission wavelengths of 490 and 520 nm, respectively. Samples were calibrated against a standard calibration curve with known amounts of hydrogen peroxide, APF, potassium phosphate buffer at pH 7.4, and HRP. APF was purchased from Invitrogen. All other chemicals were obtained from Fisher Scientific, except for Type II horseradish peroxidase, which was acquired from Sigma. All chemicals were of the

highest available purity. The SLF, hydrogen peroxide, HRP and phosphate buffer solutions were prepared in Easy Pure 18.3 MΩ-cm, UV-irradiated, ultra-filtered water and stored in the dark at 4°C.

Results

A comparison between the oxidative dissolution rates of pyrite in water versus SLF was performed on the basis of net sulfate formation per unit time. The starting SLF solution contains some sulfate, hence the comparison of oxidative dissolution rate of pyrite in SLF and water is based on the rate of sulfate formation over time, or net sulfate formation per unit time. The net sulfate formation rate is calculated based on a linear regression of sulfate concentrations determined in triplicate of samples withdrawn from the vessel over the course of the experiment. The regression analysis shows that the oxidative dissolution of pyrite in SLF is twice as slow (51%) as compared to its oxidative dissolution rate in water (Fig. 1). The addition of Survanta® has no effect on the rate of pyrite oxidative dissolution in SLF (Fig. 1). This indicates that SLF with or without fatty acids and proteins exerts an important inhibitory effect on the oxidative dissolution of pyrite.

While the oxidative dissolution rate in SLF appears to be suppressed when compared to water, the hydrogen peroxide content in SLF is nearly twice as high initially (Fig. 2). Preliminary experiments with SLF without Survanta® showed a steady state hydrogen peroxide concentration that was twice as high as the steady state concentration in an equivalent experiment with water. In the experiment with SLF presented in Fig. 2, Survanta® was added before a steady state concentration in hydrogen peroxide was established. After the addition of Survanta®, the hydrogen peroxide concentration dropped rapidly, well below the level seen in the experiment with water.

Experiments using APF show that on average the hydroxyl radical concentration was 78% higher in experiments with water compared to experiments with simple SLF (Fig. 3).

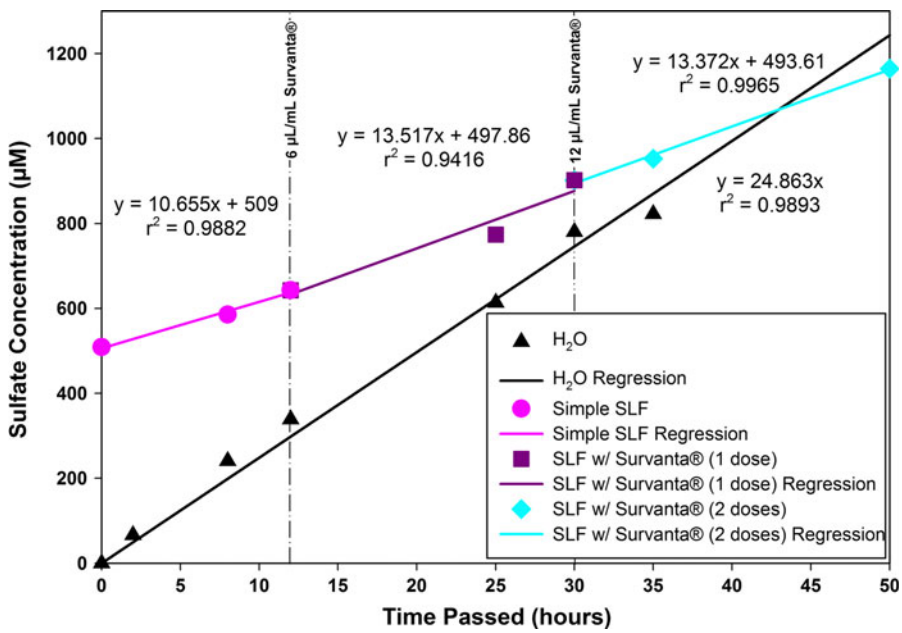

Fig. 1 Sulfate formation over time in batch experiments with pyrite. Batch oxidative dissolution experiments in which the sulfate formations between slurries of pyrite in water or SLF are compared. At two different points in time during the experiment with SLF, Survanta® was added as indicated by the *dashed vertical lines*. The temperature and pH were kept at 37°C and 7.4, respectively. Each symbol is the average concentration of triplicate analyses of sulfate; *error bars* for the average of the triplicate measurements are smaller than *symbols* used in graph. See text for more experimental details

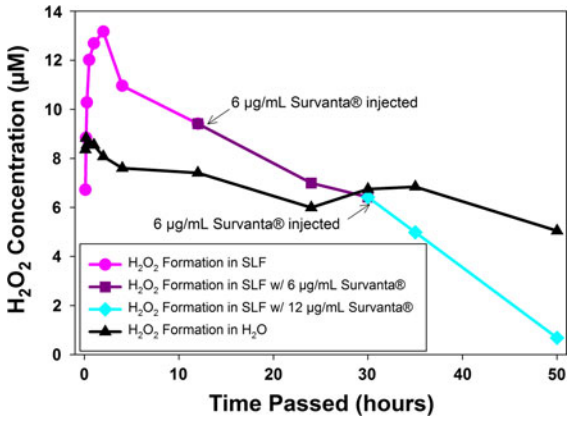

Fig. 2 Hydrogen peroxide formation/degradation over time in batch experiments with pyrite. Hydrogen peroxide concentration throughout the course of batch oxidative dissolution experiments of pyrite performed in water and SLF, respectively. Note that Survanta® was added in two separate doses in the experiment with SLF, see *arrows*

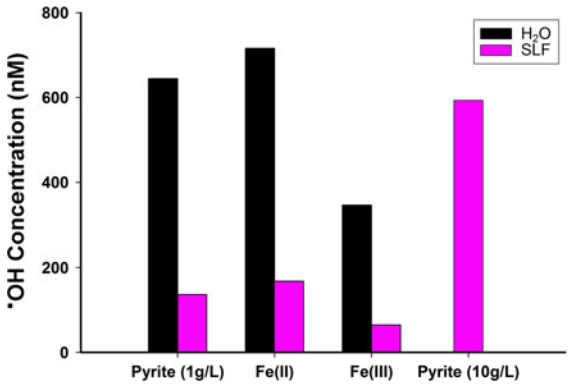

Fig. 3 Comparison of hydroxyl radical formation under a variety of conditions with water or simulated lung fluid. Fluorescence assay experiments evaluating the production of hydroxyl radicals in water and SLF without fatty acids or proteins under varying conditions. The formation of hydroxyl radicals in the experiment performed in water with a pyrite loading of 10 g/L is not represented since maximum detection limits were exceeded

Discussion

The results show a significant decrease in pyrite oxidative dissolution rate combined with a higher initial concentration of hydrogen peroxide, but a lower concentration of hydroxyl radical in SLF compared to water. The slower pyrite oxidative dissolution in SLF is not unexpected, since the presence of phosphate inhibits pyrite oxidative dissolution, particularly at pH 4 and higher (Elsetinow et al. 2001). Given the phosphate concentration in SLF (1.2 mM), one would expect a significant suppression of the oxidative dissolution rate. Besides phosphate, organic components in SLF may also contribute to the diminished oxidative dissolution rate; for instance, glycine adsorbs to sulfur defects sites on the pyrite surface (Nair et al. 2006). It is somewhat surprising that the additions of Survanta®—a natural surfactant—to simple SLF did not have an effect on the oxidative dissolution rate of pyrite, which is a surface-controlled process. However, this result is consistent with earlier work on the dissolution of talc in simple and more complex SLF (Jurinski and Rimstidt 2001). The study with talc did not show a significant difference in dissolution rate between the two conditions. Hence, the results obtained in this study indicate that the complexity of the surfactant-free SLF is sufficient to determine biopersistence of pyrite in the lungs.

The steady state concentration of hydrogen peroxide appears to be strongly influenced by the solution composition. Hydrogen peroxide is formed in the first two-electron transfer step from the pyrite surface to molecular oxygen (Schoonen et al. 2010). In addition, hydrogen peroxide is formed from superoxide when dissolved ferrous iron is oxidized by molecular oxygen. So the rate of formation of hydrogen peroxide in a pyrite slurry depends on the rate of pyrite oxidative dissolution as well as the direct one-electron reaction of molecular oxygen and dissolved ferrous iron. The steady state concentration of hydrogen peroxide is a balance between its formation and its decomposition. Hydrogen peroxide decomposition may either proceed via the Fenton reaction, which requires ferrous iron, or via a reaction with ferric iron producing water and oxygen (Schoonen et al. 2010). Hence, the amount of iron in solution and its speciation is a key factor in determining the concentration of hydrogen peroxide in these experiments at any given time.

On the basis of the stoichiometry of pyrite (FeS_2), it is expected that the rate of iron release is half that of the rate of sulfate release. For example, upon completion of the experiment performed in SLF the total concentration of sulfate was 1,165 μM, which means that the total concentration of ferrous iron released is expected to be 328 μM (this is half of the increase in sulfate over the course of the experiment, noting that 509 μM sulfate is present at the start of the

experiment because SLF contains some sulfate salt). However, the measured number was more than a factor of 10 less at 25.7 μM. This much lower dissolved iron content is a good indication that a significant amount of iron has been sequestered as Fe(III)-OH patches on the pyrite surface. The presence of these patches has been established in several studies using different techniques (Bebie et al. 1998; Ramprakash et al. 1991). Rather than passivating the pyrite surface, the Fe(III)-OH patches are known to be the major conduits for electron transfer between molecular oxygen and pyrite (Rosso et al. 1999; Jaegermann and Tributsch 1988) and are thought to play a role in the decomposition of hydrogen peroxide formed in the oxidative dissolution of pyrite (Schoonen et al. 2010). The development of the patches over time is likely responsible for the drop in hydrogen peroxide after the initial burst in the experiment with water and the section of the experiment with SLF in the absence of Survanta® (see Fig. 2).

Several components in the SLF may be influencing the relative rates of the two hydrogen peroxide decomposition reactions through complexation of dissolved iron. Earlier work has shown that hydrogen peroxide can be stabilized in pyrite slurries by adding EDTA, a strong Fe(II) chelator (Cohn et al. 2006c). Citrate, which is present in SLF used here, also forms strong complexes with ferrous iron. This notion is supported by a speciation calculation conducted with the program PHREEQCI (Parkhurst and Appelo 1999). In experiments performed in water, 98% of the ferrous iron is present as Fe^{2+}; while in experiments performed in simple SLF, 23% of the ferrous iron is present as Fe^{2+} and 64.5% is present as $FeCitrate^{-}$ (see Table 3). The high concentration of phosphate in SLF may inhibit the decomposition of hydrogen peroxide with ferric iron as reactant. This reaction is likely to take place on Fe(III)-OH patches on the pyrite surface that form as oxidative dissolution progresses. These patches are also the preferred sites for phosphate sorption. Hence, adsorption of SLF-derived phosphate is likely to slow down the decomposition of hydrogen peroxide to water and molecular oxygen. It is not clear, however, why the addition of Survanta® promotes the decomposition hydrogen peroxide (Fig. 2). The addition of Survanta® triggers a rapid decrease of the hydrogen peroxide concentration, but it remains unclear whether this is due to a decrease of hydrogen peroxide formation or an increase in its decomposition.

Table 3 Speciation of ferrous iron in SLF and H_2O

Species	Percent	
	SLF	H_2O
$FeCitrate^{-}$	64.50	–
Fe^{+2}	23.18	98.16
$FeHPO_4$	10.76	–
$FeH_2PO_4^{+}$	1.18	–
$FeOH^{+}$	0.20	1.85
$FeSO_4$	0.19	4.1×10^{-5}
$Fe(OH)_2$	8.3×10^{-5}	1.1×10^{-3}
$Fe(HS)_2$	4.5×10^{-7}	8.8×10^{-6}
$Fe(OH)_3^{-}$	1.2×10^{-7}	1.1×10^{-6}
FeCitrateH	1.2×10^{-8}	9.6×10^{-12}
$Fe(HS)_3^{-}$	5.5×10^{-13}	–

Speciation calculations performed by PHREEQCI (Parkhurst and Appelo 1999)

Chelation of ferrous iron could also explain the lower concentration of hydroxyl radical in the experiments with simple SLF. By chelating ferrous iron, the hydrogen peroxide is partially stabilized and less hydroxyl radical is formed. Another factor that is difficult to evaluate is the possibility that some hydroxyl radical may have reacted with organic components present in SLF, generating other radicals for which APF is not sensitive. For example, glycine is known to react with hydroxyl radical (Taniguchi et al. 1968; Berger et al. 1999). This reaction then may have suppressed the hydroxyl radical concentration as reported by the APF probe. The only way to evaluate this is to conduct a series of Electron Spin Resonance experiments, which would determine the type and approximate concentrations of radical(s) present. However, this is outside the scope of the present study.

The results of this research allow one to constrain the lifetime of inhaled pyrite particles and evaluate their possible role in CWP pathogenesis. On the basis of the oxidative dissolution rate of pyrite in SLF (Table 4; Fig. 1), the length of time an individual pyrite grain could be expected to persist in the lungs is determined based on the dissolution kinetics model by Lasaga (1984) (Fig. 4). Predictably, fine-grained pyrite particles will dissolve in a shorter period of time. For example, a one micron particle is expected to be dissolved in about 1.5 years. By contrast, a particle with a diameter of 10 μm is projected to take more than a decade to dissolve. Approximately 80% of the

Table 4 Lifespan of a pyrite particle based on dissolution rates for varying conditions

Experiment	Dissolution rate ($mol/m^2/s$)	Lifespan of a 1 μm pyrite particle (years)
Water	8.63×10^{-10}	0.77
"Simple" SLF	3.70×10^{-10}	1.79
SLF with 6 μg/mL Survanta®	4.69×10^{-10}	1.41
SLF with 12 μg/mL Survanta®	4.64×10^{-10}	1.43
Overall SLF[a]	4.38×10^{-10}	1.51

Experiments kept at 37°C with a pH of 7.4 and the pyrite had a specific surface area of 1.923 m^2/g and sample loading of 0.004 m^2/mL

[a] The overall dissolution rate of pyrite in "simple" SLF and the SLF after being dosed with Survanta®. The r^2 value for this line is 0.9867

airborne particles in an underground coal mine are larger than 10 μm, which is the cutoff for a particle to be considered respirable (Seixas et al. 1995). Pyrite in coal is typically present as micron or submicron particles embedded in the coal (Frankie and Hower 1987; Wiese and Fyfe 1986). So a lifespan on the basis of a one micron particle is more realistic. However, in gold and base-metal mines where pyrite is also common, the crystal size of pyrite in the rock is typically well above one micron. Hence, frequent exposure to coal dust, or other mined material, containing pyrite is expected to lead to a buildup of pyrite in the lung. The implication of the work reported here is that exposure to coal dust will lead to inhalation of pyrite particles that will slowly dissolve over the time scale of years. Research into the iron content of coal miner's pneumoconiotic lung tissue supports these timescales in that the tissue contained abnormally high amounts of iron but no pyrite (Bergman and Casswell 1972). Since autopsies usually occur years after retirement all of the pyrite should be dissolved, leaving only iron.

The persistence of respirable pyrite particles on timescales of years may promote a chronic level of inflammation with pyrite-derived hydrogen peroxide and ferrous iron producing the highly reactive hydroxyl radical. Other mineral components in coal, such as quartz, may contribute to the pathogenesis of CWP, but none of these particles produce hydrogen peroxide and hydroxyl radical in the quantities seen with pyrite (Cohn et al. 2006a). Quartz and other minerals present in coal are, however, more persistent

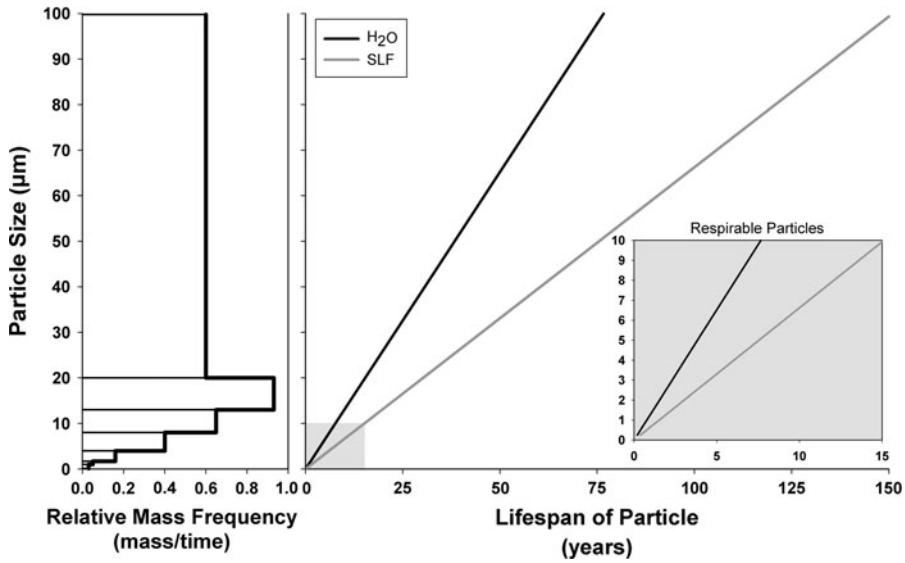

Fig. 4 Persistence of pyrite as a function of size. The lifespan of pyrite particles of varying sizes in water versus SLF based on the dissolution rates determined in this study and the calculation scheme put forth by Lasaga (1984). To place the size of the particles in the context of exposures coal miners might experience, the relative mass frequency of particles found in the air of underground coal mines is shown in the *left panel* of the figure (Seixas et al. 1995). The calculated results for pyrite particles with a size up to 10 μm are expanded in the inset on the lower right. Particles between 10 and 20 μm are abundant in air collected in active parts of underground coal mines

Table 5 Calculated mean lifetime of a 1 μm diameter particle in water

Mineral	Lifetime (years)
Quartz[a]	17,024
Forsterite[b]	302
Enstatite[c]	5.06
Pyrite	0.77
Chrysotile[d]	0.58
Anorthite[e]	0.03

Calculation scheme of Lasaga (1984) was used

[a] Rimstidt and Barnes (1980)

[b] Grandstaff (1980)

[c] Schott et al. (1981)

[d] Lifetime taken directly from Jurinski and Rimstidt (2001). Experiment in a phosphate-buffered saline solution

[e] Fleer (1982)

due to their very slow dissolution rate. This is illustrated with calculations of the lifespan of one micron particles of pyrite compared to that of one micron quartz particles (Table 5). Note that these calculations are based on dissolution rates in pure water, not SLF, so data in Table 5 represent a minimum life span. The reactivity of other minerals linked to occupational lung ailments, chrysotile (white asbestos) and forsterite (olivine; used in glassmaking), are also presented in Table 5 for comparison. One micron asbestos particles are projected to be dissolved in less than a year, while one micron forsterite and quartz particles will not be dissolved in a human lifetime. There is clearly a need to conduct dissolution experiments in SLF so that more accurate estimates of the persistence of minerals important in occupational health can be obtained.

It is important to recognize that while this study addresses some of the complexity of inhalation exposure of pyrite associated with coal; it does not take into account the contribution of cellular responses to the exposure. For example, it is well known that epithelial cells will produce hydrogen peroxide in response to exposure to particulate matter. The hydrogen peroxide produced via this cellular mechanism will be in addition to any hydrogen peroxide produced by the minerals themselves. This also raises the specter of a synergy between pyrite and biopersistent minerals, such as quartz contained in coal. Both quartz and pyrite may trigger the cells to produce hydrogen peroxide, but pyrite promotes the formation of hydroxyl radical within the cells, which can contribute to the pathogenesis of CWP. We are currently studying the cellular response of epithelial cells to exposures of coal with different levels of pyrite.

Conclusions

The oxidative dissolution rate of pyrite in SLF with or without proteins and fatty acids has been determined for the first time. The addition of proteins and fatty acids to SLF does not affect the oxidative dissolution rate. The oxidative dissolution rate in SLF is about a factor of two slower than the rate of pyrite oxidative dissolution measured in air-saturated water. Not only does the SLF lead to a slower dissolution rate, it also changes the concentration of hydrogen peroxide and hydroxyl radical in solution. Chelation of iron is thought to be responsible for the stabilization of hydrogen peroxide, leading to higher initial concentrations than in experiments with water. Over time, the concentration of hydrogen peroxide decreases; addition of beractant (Survanta®) to SLF leads to a rapid decrease of hydrogen peroxide in pyrite slurries. The initial stabilization of hydrogen peroxide also explains the lower hydroxyl radical concentrations observed in experiments with SLF. The pyrite oxidative dissolution rate data in SLF suggests that pyrite particles with a size of one micron are expected to persist for more than a year in the lung. Thus frequent inhalation exposure to pyrite can lead to the buildup of a source of reactive ferrous iron that likely contributes to the pathogenesis of CWP.

Acknowledgments The authors would like to acknowledge three independent reviewers who gave suggestions to improve the study. This work was supported by the Minerals, Metals, Metalloids and Toxicity (3MT) program at Stony Brook, directed by Schoonen. The 3MT program is funded by NSF-IGERT.

References

Bauer, J., Mattson, S. M., & Eastes, W. (1997). In vitro *acellular method for determining fiber durability in simulated lung fluid*. Unpublished report. Available electronically at: http://fiberscience.owenscorning.com/prokdis/prokdis.html.

Bebie, J., & Schoonen, M. A. A. (2000). Pyrite surface interaction with selected organic aqueous species under anoxic conditions. *Geochemical Transactions, 1*, 7.

Bebie, J., Schoonen, M. A. A., Fuhrmann, M., & Strongin, D. R. (1998). Surface charge development on transition metal sulfides: An electrokinetic study. *Geochimica et Cosmochimica Acta, 62*(4), 633–642.

Berger, P., Leitner, N. K. V., Dore, M., & Legube, B. (1999). Ozone and hydroxyl radicals induced oxidation of glycine. *Water Research, 33*(2), 433–441.

Bergman, I., & Casswell, C. (1972). Lung dust and lung iron contents of coal workers in different coal fields in Great Britain. *British Journal of Industrial Medicine, 29*(2), 160–168.

Berlinger, B., Ellingsen, D. G., Naray, M., Zaray, G., & Thomassen, Y. (2008). A study of the bio-accessibility of welding fumes. *Journal of Environmental Monitoring, 10*(12), 1448–1453. doi:10.1039/b806631k.

Cannon, G. J., & Swanson, J. A. (1992). The macrophage capacity for phagocytosis. *Journal of Cell Science, 101*, 907–913.

Cohn, C. A., Laffers, R., & Schoonen, M. A. A. (2006a). Using yeast RNA as a probe for generation of hydroxyl radicals by earth materials. *Environmental Science and Technology, 40*(8), 2838–2843. doi:10.1021/es052301k.

Cohn, C. A., Laffers, R., Simon, S. R., O'Riordan, T., & Schoonen, M. A. A. (2006b). Role of pyrite in formation of hydroxyl radicals in coal: Possible implications for human health. *Particle and Fibre Toxicology, 3*(1), 16.

Cohn, C. A., Mueller, S., Wimmer, E., Leifer, N., Greenbaum, S., Strongin, D. R., et al. (2006c). Pyrite-induced hydroxyl radical formation and its effect on nucleic acids. *Geochemical Transactions, 7*, 3–11. doi:10.1186/1467-4866-7-3.

Cohn, C. A., Pak, A., Strongin, D., & Schoonen, M. A. (2005). Quantifying hydrogen peroxide in iron-containing solutions using leuco crystal violet. *Geochemical Transactions, 6*(3), 47–51. doi:10.1063/1.1935449.

Cohn, C. A., Pedigo, C. E., Hylton, S. N., Simon, S. R., & Schoonen, M. A. A. (2009). Evaluating the use of 3′-(*p*-aminophenyl) fluorescein for determining the formation of highly reactive oxygen species in particle suspensions. *Geochemical Transactions, 10*, 8–16. doi:10.1186/1467-4866-10-8.

de Meringo, A., Morscheidt, C., Thelohan, S., & Tiesler, H. (1994). In vitro assessment of biodurability: Acellular systems. *Environmental Health Perspectives, 102*, 47–53.

Dorr, M., Kassbohrer, J., Grunert, R., Kreisel, G., Brand, W. A., Werner, R. A., et al. (2003). A possible prebiotic formation of ammonia from dinitrogen on iron sulfide surfaces. *Angewandte Chemie-International Edition, 42*(13), 1540–1543. doi:10.1002/anie.200250371.

Drugs.com. (Updated September 19, 2011; Cited September 20, 2011). Survanta. http://www.drugs.com/pro/survanta.html.

Eastes, W., Morris, K. J., Morgan, A., Launder, K. A., Collier, C. G., Davis, J. A., et al. (1995). Dissolution of glass fibers in the rat lung following intratracheal instillation. *Inhalation Toxicology, 7*(2), 197–213.

Elsetinow, A. R., Schoonen, M. A. A., & Strongin, D. R. (2001). Aqueous geochemical and surface science investigation of the effect of phosphate on pyrite oxidation. *Environmental Science and Technology, 35*(11), 2252–2257.

Fleer, V. N. (1982). *The dissolution kinetics of anorthite ($CaAl_2SiO_8$) and synthetic strontium feldspar ($SrAl_2Si_2O_8$) in aqueous solutions at temperatures below 100°C: With applications to the geological disposal of radioactive nuclear wastes*. Ph.D. thesis. University Park, PA: State University.

Frankie, K. A., & Hower, J. C. (1987). Variation in pyrite size, form, and microlithotype association in the Springfield (no-9) and Herrin (no-11) coals, Western Kentucky. *International Journal of Coal Geology, 7*(4), 349–364.

Gamble, J. L. (1942). *Chemical anatomy, physiology, and pathology of extracellular fluid: A lecture syllabus* (6th ed.). Cambridge, MA: Harvard University Press.

Grandstaff, D. E. (1980). The dissolution rate of forsterite olivine from Hawaiian beach sand. In *Proceedings on third international symposium on water–rock interaction*.

Huang, X., Fournier, J., Koenig, K., & Chen, L. C. (1998). Buffering capacity of coal and its acid-soluble Fe^{2+} content: Possible role in coal workers' pneumoconiosis. *Chemical Research in Toxicology, 11*(7), 722–729.

Huang, X., Li, W. H., Attfield, M. D., Nadas, A., Frenkel, K., & Finkelman, R. B. (2005). Mapping and prediction of coal workers' pneumoconiosis with bioavailable iron content in the bituminous coals. *Environmental Health Perspectives, 113*(8), 964–968. doi:10.1289/ehp.7679.

Jaegermann, W., & Tributsch, H. (1988). Interfacial properties of semiconduting transition metal chalcogenides. *Progress in Surface Science, 29*, 167.

Jurinski, J. B., & Rimstidt, J. D. (2001). Biodurability of talc. *American Mineralogist, 86*, 8.

Kanapilly, G. M. (1977). Alveolar microenvironment and its relationship to retention and transport into blood of aerosols deposited in alveoli. *Health Physics, 32*(2), 89–100.

Lasaga, A. C. (1984). Chemical-kinetics of water–rock interactions. *Journal of Geophysical Research, 89*(NB6), 4009–4025.

Lehuede, P., deMeringo, A., & Bernstein, D. M. (1997). Comparison of the chemical evolution of MMVF following inhalation exposure in rats and acellular in vitro dissolution. *Inhalation Toxicology, 9*(6), 495–523.

Mattson, S. M. (1994). Glass fiber dissolution in simulated lung fluid and measures needed to improve consistency and correspondence to in vivo dissolution. *Environmental Health Perspectives, 102*, 87–90.

Metzger, R., Wichers, D., Vaselin, J., & Velasquez, P. (1997). Solubility characterization of airborne uranium from an in situ uranium processing plant. *Health Physics, 72*(3), 418–422.

Morrow, P. E. (1988). Possible mechanisms to explain dust overloading of the lungs. *Fundamental and Applied Toxicology, 10*(3), 369–384.

Nair, N. N., Schreiner, E., & Marx, D. (2006). Glycine at the pyrite-water interface: The role of surface defects. *Journal of the American Chemical Society, 128*(42), 13815–13826. doi:10.1021/ja063295a.

NIOSH. (2003). *Work-related lung disease surveillance report 2002*. Cincinnati, OH: National Occupational Safety and Health.

Oberdorster, G. (1995). Lung particle overload: Implications for occupational exposures to particles. *Regulatory Toxicology and Pharmacology, 21*(1), 123–135.

Oze, C., & Solt, K. (2010). Biodurability of chrysotile and tremolite asbestos in simulated lung and gastric fluids. *American Mineralogist, 95*(5–6), 825–831. doi:10.2138/am.2010.3265.

Parkhurst, D. L., & Appelo, C. A. J. (1999). User's guide to PHREEQC (Version 2)—A computer program for speciation, batch-reaction, one-dimensional transport, and inverse geochemical calculations. *U.S. Geological Survey Water-Resources Investigations Report, 99*(4259), 1.

Potter, R. M., & Mattson, S. M. (1991). Glass-fiber dissolution in a physiological saline solution. *Glastechnische Berichte-Glass Science and Technology, 64*(1), 16–28.

Ramprakash, Y., Koch, D. F. A., & Woods, R. (1991). The interaction of iron species with pyrite surfaces. *Journal of Applied Electrochemistry, 21*(6), 531–536.

Renwick, L. C., Donaldson, K., & Clouter, A. (2001). Impairment of alveolar macrophage phagocytosis by ultrafine particles. *Toxicology and Applied Pharmacology, 172*(2), 119–127.

Rimstidt, J. D., & Barnes, H. L. (1980). The kinetics of silica–water reactions. *Geochemical Cosmochemical Acta, 44*, 17.

Rosso, K. M., Becker, U., & Hochella, M. F. (1999). The interaction of pyrite 100 surfaces with O^{-2} and H_2O: Fundamental oxidation mechanisms. *American Mineralogist, 84*, 13.

Schoonen, M. A. A., Elsetinow, A. R., Borda, M., & Strongin, D. R. (2000). Effect of temperature and illumination on pyrite oxidation between pH 2 and 6. *Geochemical Transactions, 1*, 23. doi:10.1039/b004044o.

Schoonen, M. A. A., Harrington, A. D., Laffers, R., & Strongin, D. R. (2010). Role of hydrogen peroxide and hydroxyl radical in pyrite oxidation by molecular oxygen. *Geochemical Cosmochemical Acta, 74*(17), 4971–4987.

Schott, J., Berner, R. A., & Sjoberg, E. L. (1981). Mechanism of pyroxene and amphibole weathering, I. Experimental studies of iron-free minerals. *Geochemical Cosmochemical Acta, 45*, 13.

Seixas, N. S., Hewett, P., Robins, T. G., & Haney, R. (1995). Variability of particle size-specific fractions of personal coal-mine dust exposures. *American Industrial Hygiene Association Journal, 56*(3), 243–250.

Taniguchi, H., Fukui, K., Ohnishi, S., Hatano, H., Hasegawa, H., & Maruyama, T. (1968). Free-radical intermediates in the reaction of the hydroxyl radical with amino acids. *The Journal of Physical Chemistry, 72*(6), 1926–1931. doi:10.1021/j100852a012.

USEIA. (2009). International Energy Outlook. http://www.eia.doe.gov/oiaf/ieo/highlights.html, DOE/EIA-0484.

USEIA. (2011). What is the role of coal in the United States? Engery in brief—What everyone should know about energy. http://www.eia.gov/cfapps/energy_in_brief/role_coal_us.cfm.

Wang, L. Y., Castranova, V., Mishra, A., Chen, B., Mercer, R. R., Schwegler-Berry, D., et al. (2010). Dispersion of single-walled carbon nanotubes by a natural lung surfactant for pulmonary in vitro and in vivo toxicity studies. *Particle and Fibre Toxicology, 7*. doi:10.1186/1743-8977-7-31.

Wiese, R. G., & Fyfe, W. S. (1986). Occurences of iron sulfides in Ohio coals. *International Journal of Coal Geology, 6*(3), 251–276.

Wragg, J., & Klinck, B. (2007). The bioaccessibility of lead from Welsh mine waste using a respiratory uptake test. *Journal of Environmental Science and Health Part A-Toxic/Hazardous Substances & Environmental Engineering, 42*(9), 1223–1231. doi:10.1080/10934520701436054.